Received: 31 May 2021 | Revised: 8 November 2021 | Accepted: 7 December 2021

DOI: 10.1002/hyp.14472

RESEARCH ARTICLE

WILEY

New insights into particle transport in karst conduits using comparative tracer tests with natural sediments and solutes during low-flow and high-flow conditions

Dominik Richter | **Nadine Goeppert** | **Nico Goldscheider**

Karlsruhe Institute of Technology (KIT), Institute of Applied Geosciences, Division of Hydrogeology, Karlsruhe, Germany

Correspondence
Dominik Richter, Karlsruhe Institute of Technology (KIT), Institute of Applied Geosciences, Division of Hydrogeology, Kaiserstr. 12, 76131 Karlsruhe, Germany.
Email: dominik.richter@kit.edu

Funding information
Bundesministerium für Bildung und Forschung, Grant/Award Number: 02WCL1415

Abstract

Colloidal particles are an important vector for the transport of contaminants in karst aquifers, characterized by a high degree of hydrologic variability. Understanding this heterogeneity and hydrogeological functioning is of particular importance for water management strategies. Until now, transport parameters for particles were mostly determined by injection of solutes or surrogates for natural sediments. But suspended particles are easier to analyse, less expensive and better represent natural conditions. Therefore, tracer tests with sediments represent natural transport and a conservative solute dye were conducted simultaneously in an active and partly accessible cave system in Vietnam during constant high-flow and low-flow conditions. Breakthrough curves (BTCs) for 10 different particle sizes classes ranging from 1 to 15 μm and the solute were recorded in situ at the two main resurgences of the cave stream at high temporal resolution. This study gives new insights into the transport processes of suspended particles and the highly dynamic exchange between mobile and immobile regions. Major findings include: (1) at low-flow conditions, inflow from the surrounding aquifer matrix and the velocity distribution inside the karst conduits themselves lead to hydrodynamic focusing, mainly affecting particles; (2) this highly advective, preferential transport of particles in the centre of the karst conduits results in narrow BTC. The more dispersive transport of solutes results in a longer tailing; (3) at high-flow conditions a more homogeneous distribution of the particles indicates a reversal of the conduit-matrix interaction; (4) by comparing the results at different hydraulic conditions, the activation of additional flow paths with increasing discharge could be identified. This study also presents the first tracer test in the field resulting in pronounced double peaks for the particulate tracer but only a single, right-skewed BTC for the simultaneously injected solute, including a conceptual model for particle transport.

KEYWORDS
conservative tracer, hydrodynamic focussing, karst aquifer, particle transport

1 | INTRODUCTION

Karst aquifers are characterized by large fissures and large conduit apertures, leading to long travel distances of suspended particles with high flow velocities. This rapid flow through the karst aquifer makes them prone to transport of particulate matter (e.g., Pronk et al., 2009). The potentially high mobility of suspended particles in karst aquifers has to be taken into account for water management, predicting the behaviour of contaminants and understanding the natural distribution of chemicals and bacteria in the aquifer (e.g., Ryan & Meiman, 1996; Schiperski et al., 2016). Therefore, a profound understanding of particle transport in karst aquifers is of crucial importance.

Particles are omnipresent in surface water and karst aquifers. They have been pointed out as vectors for pollutant transport because they can act as sorbents towards pathogens or other hydrophobic contaminants (e.g., Mahler et al., 2004; McCarthy & Zachara, 1989; Vuilleumier, 2017). Anthropogenic pollutants, such as heavy metals, are mainly adsorbed onto suspended particulates (Vesper & White, 2003). Bacteria tend to adhere to particles; free-floating bacteria are less persistent within the aquatic environment (Dussart-Baptista et al., 2003; Pronk et al., 2006; Schillinger & Gannon, 1985). Mahler et al. (2000) observed, that bacteria are likely be mobilized together with fine sediments; therefore, large proportions of faecal bacteria in karst aquifers are associated with suspended sediments.

Furthermore, karst terranes are often characterized by scarce soils and serious erosion. Due to rapid infiltration through the epikarst and very low filtration and storage capacities, karst aquifers are highly vulnerable to the input of these eroded sediments and their associated pollutants from the land surface (e.g., Bakalowicz, 2005; Rügner et al., 2019; Schiperski et al., 2015). Additionally, autogenic sediments are released during carbonate rock dissolution and are transported in the conduit network (Dreybrodt, 1996; Pronk et al., 2006).

Suspended sediments in surface streams and groundwater can also cause an environmental risk in terms of ecological water quality. High-suspended sediment loads increase turbidity which affects aquatic life (Carling & McCahon, 1987; Davies-Colley et al., 1992). The organic parts of the suspended solids cause oxygen depletion with their decomposition by microorganisms and thus harm the flora and fauna of water bodies (Hillebrand, 2008).

The mechanisms and characteristics of particle transport in karst aquifers have been investigated in several field studies with fluorescent polystyrene microspheres (Goeppert & Goldscheider, 2008; Schiperski et al., 2016), biological tracers such as bacteriophages (Auckenthaler et al., 2002; Flynn & Sinreich, 2010), and bacteria (Sinreich et al., 2009) as surrogates for colloidal particles.

However, the behaviour of these particles cannot be transferred in their entirety to natural particles that are normally present in the aquifer. Furthermore, the application of chemicals as tracers has several restrictions as toxicity, visibility or costs and are not globally to be obtained compared to sediments.

For an improved understanding of the transport properties of natural suspended particles, Goeppert and Goldscheider (2019) injected sediment particles as an artificial, particulate tracer simultaneously with a solute dye tracer into a swallow hole and monitored the breakthrough curves (BTCs) at a karst spring. The results of this study show that sediment particles can be used efficiently as an artificial tracer in the alpine benchmark site and highlight the different transport behaviours of solute and particulate transport in karst conduits.

Large parts of karst areas are located in subtropical or tropical regions with distinct dry and rainy seasons (Goldscheider et al., 2020), and big rain events can have a large impact on the transport of suspended particles (Pronk et al., 2009). Thus, the objectives of this study were (a) to assess the impact of different hydrologic conditions on the particulate transport processes of natural sediments in karst aquifers, (b) to compare the transport of particles and solutes, and (c) to study the impact of particle sizes on the flow and transport parameter.

The aim is to gain a deeper understanding of the processes and mechanisms of particulate transport in karst aquifers. This knowledge about deposition behaviour of fine sediments in combination with information on particle-bound contaminants can be used to improve forecasts, to better assess factors influencing sediment transport processes, and can help to improve the management of karst groundwater resources.

2 | MATERIALS AND METHODS

2.1 | Test site and general experimental test setup

The experimental test site is located in the northernmost Vietnamese province Ha Giang (Figure 1a). Non-karstified Devonian silty limestone and schists interbedded with sandstone dip southwest under a Carboniferous-Permian karst formation. In the test site, the surface stream Ma Le River sinks underground into a 1.492 m long cave system at the boundary of these two formations (Figure 1b). The cave system consists of the swallow hole Ma Le 1 (ML 1), two cave sections with phreatic zones in between an open channel flow, a separate entrance chamber facilitating access to each (ML 2 and ML 3), and the two resurgences of the cave stream ML 4 and Seo Ho 1 (SH 1) forming the Seo Ho River (Figure 1). Ender et al. (2018) provided evidence of a connection from the swallow hole to the two resurgences of the cave stream with a fluorescent dye tracer. Furthermore, their results show, that the cave system does not only have a single cave stream. The stream can be divided into several contributaries. The contributaries vary in quantity and their relative proportions based on the hydrologic conditions. Depending on the discharge rates additional flow paths could be activated.

The Belgian caving club SPEKUL explored large sections of the cave system except the phreatic zones. The hydraulic gradient of the three cave sections ML 1 to ML 3 decreases along the flow direction from 11% (ML 1) over 5% (ML 2) to 2% (ML 3) (Lagrou, unpublished report, 2005). The cave section from ML 3 to ML 4/SH 1 is not accessible. But since the discharge of SH 1 is almost constant at all hydraulic conditions and the rates of ML 4 vary distinctly, it can be assumed,

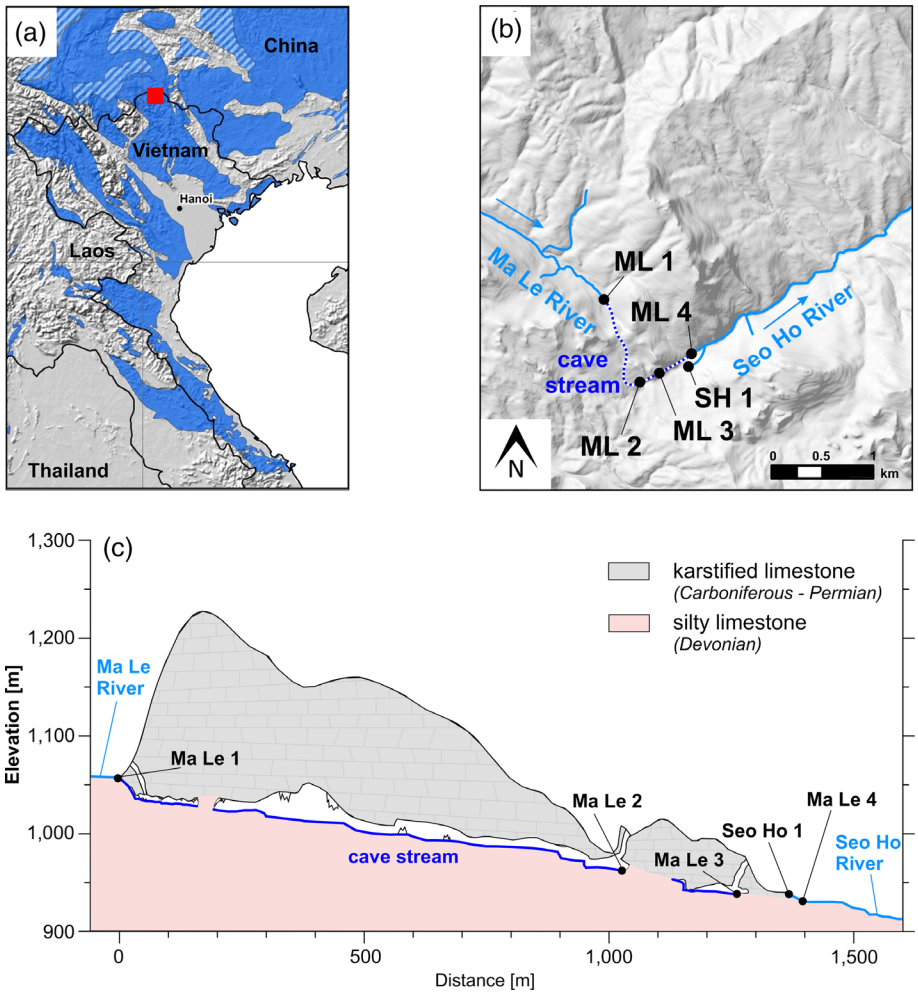

FIGURE 1 (a) Location of the study site on an excerpt from the world karst aquifer map (Goldscheider et al., 2020); distribution of carbonate rocks in Vietnam and adjacent countries in blue; test site is highlighted with a red square. (b) Surface streams and the known cave stream, and sampling sites. (c) Cross-section, following the course of the caves (modified after Ender et al., 2018) with the sampling sites Ma Le 3 (ML 3), Ma Le 4 (ML 4), and Seo Ho 1 (SH 1)

TABLE 1 Tracer tests conducted in the Ma Le cave system; n.m. not measured

		Sampling			
Conditions	**Injection mass**	**ML 1**	**ML 3**	**SH 1**	**ML 4**
Low-flow	Uranine: 50 *g* Particles: 3.62×10^{14} n	Injection	Particles: *manually* Uranine: *Field fluorimeter* Discharge: 168 ± 6 L/s	Particles: *PCSS fluid lite* Uranine: *manually* Discharge: 28 ± 1 L/s	Particles: *PCSS fluid lite* Uranine: *field fluorimeter* Discharge: 132 ± 5 L/s
High-flow	Uranine: 60 g Particles: 5.47×10^{14} n	Injection	n.m.	Particles: *PCSS fluid lite* Uranine: *manually* Discharge: 23 ± 1 L/s	Particles: *PCSS fluid lite* Uranine: *field fluorimeter* Discharge: 986 ± 13 L/s
	Distance from injection		1.314 m	1.454 m	1.492 m

that ML 4 acts as an overflow spring (Table 1). As the flow velocities to ML 4 and SH 1 are very similar, the branch-off to the two springs must be located nearby.

The tracer tests with particulate and dissolved tracers were carried out in both the rainy season and the dry season. Table 1 summarizes the surrounding conditions of the two tests (input quantities, sampling sites, discharge, distances). The discharge at every sampling site was measured with the salt-dilution method several times while conducting the tracer tests (Groves, 2007). During the tracer tests hydrologic conditions were constant, so interpretations of the data due to variable discharge can be excluded. For the tracer test, 50 g (low-flow) and 60 g (high-flow) uranine were used.

To ensure comparability between the two tracers used, the same method was applied for injection: Particles and uranine were diluted with river water in a tub (270 L) and injected instantaneous Dirac-like in the swallow hole ML 1. To rule out coagulation of particles in the tracer mixture, particles and uranine were injected with a time lag of 25 min. To our best of knowledge, no other relevant natural or artificial input of sediments into the studied sinking stream and cave stream occurred during the time of the experiments.

2.2 | Conservative tracer

The fluorescent dye uranine (AppliChem GmbH, Darmstadt, Germany) was used as conservative tracer. The solubility of uranine is very high; the detection limit is extremely low (≈ 0.005 μg/L), and it is harmless for humans and the environment (Behrens et al., 2001). The input mass was adapted to the seasonal discharge (Table 1). For an onsite analysis, online field fluorimeters GGUN-FL30 (Albillia Co., Neuchatel, Switzerland) with optics for uranine and turbidity were used. Additionally, water samples were collected manually in 50 ml brown glass bottles and stored in the dark at 4°C until analysis. On site, the samples were analysed using the portable field fluorimeter Trilogy (Turner Design, California) following standard procedures (Käss, 2004). Selected samples were transported to Germany and measured with a LS55 fluorescence spectrometer (Perkin Elmer Inc., Waltham) for reference. The measurement results from the laboratory confirm the measured tracer concentrations on site. All fluorimeters were calibrated using local water from the sampling locations. The calibrations for all used devices resulted in a R^2 of 0.99, the residuals were below 1%. The measurement intervals of the field fluorimeter were 30 s; for manual sampling, these intervals were adjusted.

2.3 | Sediment particles

In order to replicate the process of soil erosion most realistically, local fine sediments, collected in the catchment of the swallow hole, were used as particulate tracers. Before injection, the sediments were suspended. Input numbers and particle-size distribution (PSD) were determined by using a portable particle counter (PCSS fluid lite, Klotz GmbH, Bad Liebenzell, Germany) after dilution of 1 ml suspension and sonication for 60 s in an ultrasonic bath. The input numbers were adapted to the seasonal discharge (Table 1). To avoid sedimentation and aggregation in bottles, particle concentration was measured in situ. For this study, a rinsing cycle of 10 ml and subsequent measurement of 10 ml every 90 s was performed. The size classes for measurements are adjustable, ranging from 1 to 450 μm. Before starting the measurement series, all particle counters used were calibrated with latex spheres. This study focuses on particles up to a diameter of 15 μm. Only little variations for concentrations of particles in this range were found beforehand at the sampling point and the injection point. The background noise of particle concentrations at the sampling sites was subtracted according to Goeppert and Goldscheider (2019).

For logistical reasons (remote area, cave system) the in situ particle concentrations at low-flow conditions were measured up to 10.5 h after the injection, when the important parts of the particles breakthrough were completed. The particle data from this time on are based on a correlation with the measured turbidity of the field fluorimeters. This correlation was carried out separately for each particle-size class (PSC); the coefficient of determination for particles up to 15 μm diameter ranges from 0.94 to 0.99. At high-flow conditions, the coincidence level of the sensor was exceeded for 16 measurements (only 1–4 μm). For sampling site ML 4 these data were also extrapolated based on the established correlation between turbidity and individual particle-size classes (R^2 ranging from 0.94–0.97). Since there is no turbidity signal for SH 1 at high-flow, the model for this site is calculated without these 16 data points.

2.4 | Data analyses and modelling

To simplify comparison, all BTCs were normalized by dividing the measured concentrations by the injected mass (for uranine), of the number of particles (for the particulate tracer), as it levels out the effect of different tracer types and input quantities (Käss, 2004). Basic transport parameters for uranine and each particle-size class were calculated directly from the BTCs. These robust parameters include the time of first detection (t_1), and the peak concentration time (t_p), with the corresponding maximum flow velocity (v_{max}) and peak velocity (v_p). By integration of the BTCs, the recovery rates (R) for the tracers were calculated as follows:

$$R = \frac{1}{M}\int_{t=0}^{t_{end}} (Q * C)dt \quad (1)$$

where M is the injected tracer quantity (mass or particle number), Q is the discharge, and C is the (solute or particle) concentration at time t (Leibundgut et al., 2009). For the determination of further transport parameters, the software Stanmod (CXTFIT code; Toride et al., 1999) was used. The transport of the tracers can thereby be described with a one-dimensional (1D) analytical solution. This simplification is justified as flow in karst conduits is mainly one-dimensional in the direction of flow and thus dispersion and advection are most dominant in this direction. Several BTCs show a skewness in the form of a distinct tailing. Therefore, the two-region nonequilibrium (2RNE) model, originally developed to describe the exchange between mobile and immobile fluid regions as a first-order mass transfer process, was applied (Toride et al., 1993).

As it has been described in an earlier study of Ender et al. (2018) a higher coefficient of determination was obtained with the nonlinear least-square fitting procedure of the 2RNE model than by simulating the BTC with the advection-dispersion-equation.

The four parameters advection (expressed as mean flow velocity v_m), longitudinal dispersion (D), distribution coefficient β, and mass transfer coefficient ω were fitted, while the remaining parameters retardation and degradation were kept constant. The distribution coefficient β ($0 < \beta < 1$) indicates the proportion of mobile fluid within the aquifer, and the mass transfer coefficient ω ($\omega > 0$) quantifies the exchange rate between mobile and immobile regions. This model has been successfully applied to characterize tracer tests in karst aquifers (e.g., Field & Pinsky, 2000). Despite accounting for mobile and immobile fluid regions, the shape of right-skewed BTCs can also result from a combination of two or more peaks caused by dominating components of turbulent flow in the centre of conduits and laminar flow along the margins of conduits (Massei et al., 2006), variable flow rates

or length along different flow paths, or multiple flow paths (Field & Leij, 2012). For the BTCs with a double peak, a multi-dispersion model was applied (Käss, 2004; Leibundgut et al., 2009). A stepwise determination of the transport parameters needs to be realized for modelling multiple peaks with CXTFIT code. First, the earliest peak is fitted, then this fit is subtracted from the BTC. These residual concentrations are used for further fitting. Summing up the individual models yields the wrapped curve (Figure 2). Since each peak has a pronounced tailing and the background concentration is almost reached between the two peaks, the 2RNE model was used. This approach provides a much higher coefficient of correlation than the advection-dispersion equation.

3 | RESULTS

3.1 | Tracer tests at low-flow conditions

The BTCs for the solute tracer and the particulate tracer at low-flow conditions are visualized in Figure 3. The descriptive and modelled transport parameters are listed in Table 2 for ML 4, for ML 3 in Data S1 A-2, and for SH 1 in Data S1 A-3.

All three BTCs for uranine have a distinct tailing and show only one peak. Uranine was first detected in ML 3 after 2.22 h, in ML 4 and SH 1 simultaneously 1 h later. The total recovery rates at the springs (ML 4: 58.6% and SH 1: 13.9%) indicate that they are the main resurgences of the cave stream (Table 2). By applying a 2RNE model, the mean flow velocity from the swallow hole ML 1 to the karst spring ML 4 is calculated as 245 m/h for uranine (Table 2).

The results of the tracer test at low-flow conditions demonstrate transport of suspended particles up to 15 µm in diameter through the Ma Le cave system. Particularly remarkable are the narrow but pronounced double peaks, which were detected at all three sampling sites for all PSCs and turbidity. Since no other known input of sediments occurred during the experiment, we suppose that these double peaks results from the single injection of suspended sediments and the subsequent transport processes in the karst system. Therefore, all transport parameters were calculated for both peaks and are listed separately in tables (Table 2 and A-2, A-3 in Data S1).

At the resurgences of the cave stream (ML 4, SH 1), the maximum concentration of the first particle peak was detected 4.64–4.72 h after injection, and the maximum of the second peak after 8.94–9.17 h. The mean flow velocity in the first peak is constant for all size classes at the sampling sites ML 3 and SH 1, while at ML 4 mean flow velocity decreases slightly starting with a particle diameter larger than 9 µm (Figure 4). The highest mean flow velocity was determined for sampling location ML 3 (349–356 m/h). The mean flow velocities of the second peak are distinctly slower. At all three sampling sites, the recoveries decrease with increasing particle size. Corresponding to the different discharges, the highest recoveries were found at ML 3, the lowest at SH 1 (Figure 4). A linear Pearson's correlation proves the trend of decreasing dispersion with increasing particle diameter, with statistical significance for the first particle peak at the two sites ML 4 and SH 1 (Figure 4). For the second peak, the model calculated lower dispersions at all sampling sites, regardless of the particle diameter.

The recovery for the dissolved tracer is greater than for the injected particles at all sampling sites. But the mean flow velocities of all PSCs are higher than for uranine (Figure 4). All three BTCs of the solute tracer show pronounced tailings, assuming partly active bypasses and retention from mobile to immobile fluid regions (Dewaide et al., 2016). As there are two individual peaks observed for the BTCs of the particles, and the hydraulic conditions were constant throughout the tracer test, at least two flow channels or pathways in the karst system can be assumed (Goldscheider et al., 2008; Leibundgut et al., 2009).

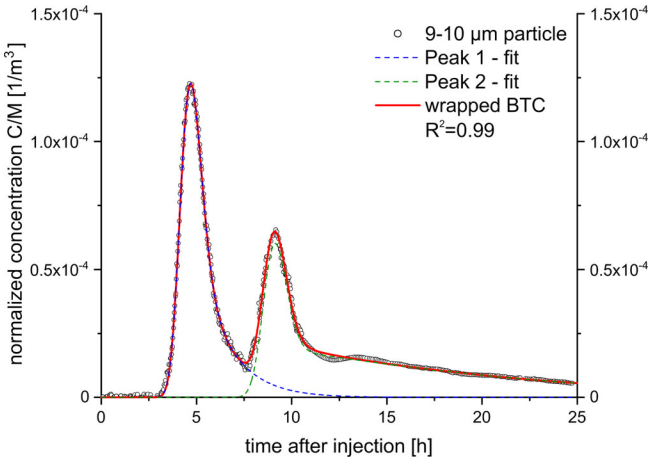

FIGURE 2 Observed and modelled BTCs (2RNE model) of particles (9–10 µm) with two individual peak fits and wrapped modelled concentrations obtained by superposition. Normalized concentrations were obtained by dividing the concentrations C by the input quantity M (particle number)

3.2 | Tracer tests at high-flow conditions

The BTCs for the solute tracer and the particulate tracer at high-flow conditions are visualized in Figure 3. The descriptive and modelled transport parameters are listed in Data S1 A-1.

Both BTCs for uranine are asymmetric right-skewed and show only one peak. Uranine was first detected in ML 4 0.87 h after injection, in SH 1 a few minutes later after 0.98 h. By applying a 2RNE model, mean flow velocity from the swallow hole ML 1 to the karst spring ML 4 is calculated with 11 515 m/h for uranine at high-flow conditions (A-1 in Data S1), indicating a well-developed karst network.

The BTCs of the particles at high-flow conditions have to be considered in a somewhat differentiated way. In contrast to low-flow conditions, at high-flow all PSCs show only a single peak with pronounced tailing. This single peak occurs between 1.10 and 1.31 h after the injection at ML 4, at SH 1 1.44 h after injection. The mean flow velocity at sampling site ML 4 decreases with increasing particle

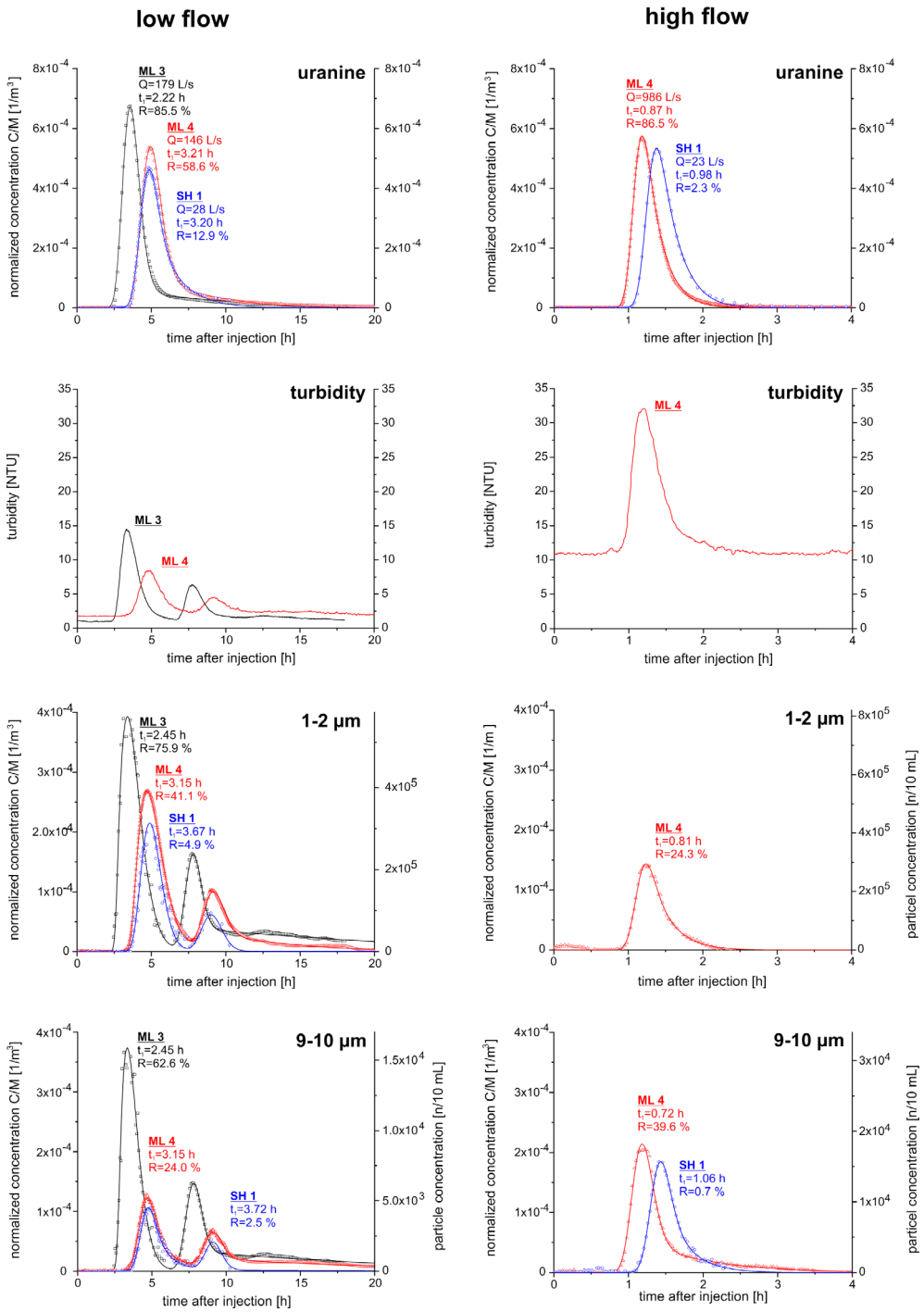

FIGURE 3 Observed (dots) and modelled (lines) BTCs of uranine, turbidity, and selected particle-size classes at high and low-flow conditions. Only the wrapped BTCs are shown. Normalized concentrations were obtained by dividing the concentrations C by the input mass (uranine), respectively input number (particles) M

size (Figure 4). The smallest particles (1–2 µm) are transported through the karst system with a mean flow velocity of 1082 m/h, whereas the largest particles (10–15 µm) are transported only with 855 m/h. The recovery of the suspended particles also depends strongly on their size. At ML 4 only 24.3% of the smallest particles (1–2 µm) could be detected. Up to a diameter of 3–4 µm, the recovery increases to 40.4% and decreases again to 20.2% up to the maximum detectable size class of 10–15 µm. Due to the considerably smaller discharge, the percentages of recoveries are lower at SH 1. Pearson's test proves linear correlation of increasing dispersion with increasing PSC with statistical significance at the two sites ML 4 and SH 1 (Figure 4).

At high-flow conditions, both recoveries and mean flow velocities are greater for the solute tracer than for the injected particles (Figure 4). The high velocities of the tracers of >1000 m/h are a clear indication that the cave stream consists of a well-developed network of karst conduits, which allow a channelled and rapid transport of dissolved substances at high discharge conditions (Goldscheider & Drew, 2007).

TABLE 2 Descriptive and modelled parameters of the two-region non-equilibrium model (2RNE) for the solute tracer uranine and the particle-size classes from 1 to 15 μm at the sampling site Ma Le 4 at low-flow conditions

	Units	Uranine	1–2 μm		2–3 μm		3–4 μm		4–5 μm		5–6 μm	
			First peak	Second peak	First peak	Second peak	First peak	Second peak	Firstpeak	Second peak	First peak	Second peak
Descriptive parameters												
M	(g)/(n)	50	1.44×10^{14}		9.13×10^{13}		4.72×10^{13}		2.72×10^{13}		1.78×10^{13}	
t_1	(h)	3.21	3.15		3.15		3.15		3.15		3.15	
v_{max}	(m/h)	465	474		474		474		474		474	
t_p	(h)	4.70	4.72	8.94	4.72	8.94	4.72	8.94	4.69	9.09	4.64	9.07
v_p	(m/h)	317	316	166	316	166	316	166	318	164	322	164
R	(%)	58.6 ± 5.9	41.1 ± 4.1		37.3 ± 3.7		29.9 ± 3.0		25.9 ± 2.6		25.2 ± 2.5	
Modelled parameters												
v_m	(m/h)	245 ± 1	289 ± 1	127 ± 1	290 ± 1	110 ± 1	291 ± 1	119 ± 1	291 ± 1	128 ± 1	292 ± 1	118 ± 1
D	(m^2/h)	3382 ± 23	3005 ± 174	546 ± 16	2987 ± 241	357 ± 15	2957 ± 33	412 ± 27	2945 ± 90	483 ± 18	2941 ± 89	410 ± 22
α	(m)	13.8 ± 0.1	10.4 ± 0.6	4.3 ± 0.1	10.3 ± 0.8	3.2 ± 0.2	10.3 ± 0.5	3.5 ± 0.3	10.1 ± 0.3	3.8 ± 0.2	10.1 ± 0.3	3.5 ± 0.2
β	(–)	0.80 ± 0.01	0.84 ± 0.01	0.79 ± 0.01	0.91 ± 0.01	0.67 ± 0.01	0.91 ± 0.01	0.73 ± 0.01	0.91 ± 0.01	0.79 ± 0.01	0.91 ± 0.01	0.72 ± 0.01
ω	(–)	0.41 ± 0.01	2.14 ± 0.28	0.75 ± 0.01	0.86 ± 0.32	1.20 ± 0.01	0.86 ± 0.12	0.91 ± 0.02	0.72 ± 0.07	0.71 ± 0.01	0.76 ± 0.08	0.93 ± 0.01
P_e	(–)	108	143	348	145	461	145	429	147	395	148	428
R^2	(–)	0.99	0.99		0.99		0.99		0.99		0.99	

		6–7 μm		7–8 μm		8–9 μm		9–10 μm		10–11 μm		11–15 μm	
		First peak	Second peak	First peak	Second peak	First peak	Second peak	First peak	Second peak	First peak	Second peak	First peak	Second peak
Descriptive parameters													
M	(g)/(n)	1.11×10^{13}		7.30×10^{12}		5.27×10^{12}		4.25×10^{12}		1.29×10^{12}		3.86×10^{12}	
t_1	(h)	3.17		3.17		3.17		3.15		3.17		3.12	
v_{max}	(m/h)	471		471		471		474		471		478	
t_p	(h)	4.69	9.14	4.69	9.12	4.69	8.96	4.67	9.12	4.74	9.17	4.67	9.07
v_p	(m/h)	318	163	316	164	318	167	319	164	315	163	321	164
R	(%)	24.1 ± 2.4		23.5 ± 2.4		23.6 ± 2.4		24.0 ± 2.4		19.7 ± 2.0		19.8 ± 2.0	
Modelled parameter													
v_m	(m/h)	290 ± 1	114 ± 1	288 ± 2	108 ± 1	285 ± 4	99 ± 1	276 ± 8	88 ± 1	263 ± 10	115 ± 2	258 ± 11	102 ± 2
D	(m^2/h)	2901 ± 86	402 ± 19	2882 ± 84	373 ± 17	2899 ± 79	337 ± 15	2886 ± 129	294 ± 15	2863 ± 101	436 ± 35	2861 ± 97	403 ± 30
α	(m)	10.0 ± 0.3	3.5 ± 0.2	10.0 ± 0.4	3.5 ± 0.2	10.2 ± 0.4	3.4 ± 0.2	10.5 ± 0.8	3.4 ± 0.2	10.9 ± 2.9	3.8 ± 0.4	11.1 ± 3.3	4.0 ± 0.4
β	(–)	0.91 ± 0.01	0.70 ± 0.01	0.91 ± 0.01	0.66 ± 0.01	0.90 ± 0.01	0.60 ± 0.01	0.88 ± 0.02	0.54 ± 0.01	0.84 ± 0.07	0.71 ± 0.01	0.82 ± 0.07	0.63 ± 0.01
ω	(–)	0.69 ± 0.07	0.98 ± 0.01	0.62 ± 0.06	1.08 ± 0.01	0.54 ± 0.05	1.22 ± 0.01	0.54 ± 0.05	1.40 ± 0.01	0.58 ± 0.03	0.76 ± 0.01	0.64 ± 0.04	0.89 ± 0.01
P_e	(–)	149	424	149	431	146	437	142	444	137	392	134	376
R^2	(–)	0.99		0.99		0.99		0.99		0.99		0.99	

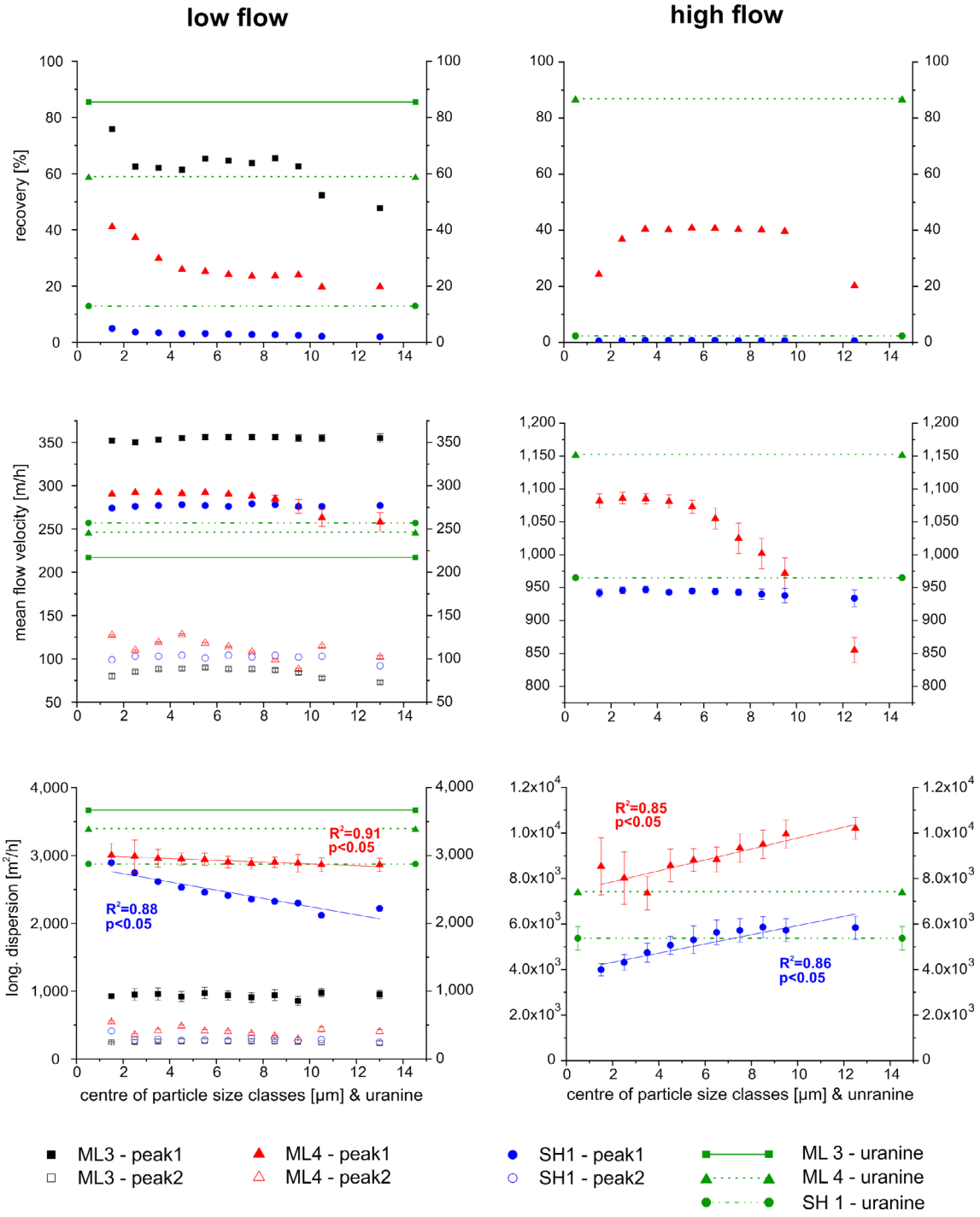

FIGURE 4 Recovery, mean flow velocities, and dispersion with *SD* for uranine and particle-size classes at low (left) and high (right) flow conditions. Trend lines are given for the particulate transport with the coefficient of determination R^2, which indicates a fair correlation. Pearson's correlation *p*-values demonstrate statistical significance. The parameters for sampling site SH 1 at high-flow conditions of the particle-size classes 1–4 µm are modelled without the data over the coincidence level. The values of uranine are shown as horizontal lines

4 | DISCUSSION

4.1 | Conceptual model of solute and particle transport at low-flow

In karst systems, the groundwater flow in the phreatic zone is mostly concentrated in often highly conductive conduits (Chen et al., 2017). The fissure and cavity geometry in karst has a high impact on suspended particles on the frictional losses at the edges of these karst conduits (Massei et al., 2006). Hence, the largest flow velocities prevail in the centre of the conduits (Gale, 1984). Central streamlines result in faster velocities and straighter paths (Keller et al., 2004).

Depending on the distribution of the hydraulic heads within the karst aquifer, the conduits exchange water with the adjacent matrix.

Stable low-flow conditions often cause water to flow from the surrounding matrix into the conduits (Frank et al., 2019). Therefore, the drainage from the matrix to the conduit and the velocity distribution may lead to a hydrodynamic focusing of the transported particles. The particles are not homogeneously transported in the entire conduit, but are mainly concentrated in the centre with the highest flow velocities and thus have less diverse flow paths (Figure 5a,b). Additionally, larger particles are affected by sedimentation processes, leading to a decreasing recovery with increasing particle diameter. Sedimentation might also influence the decreasing dispersion with increasing particle size.

As already highlighted by Keller et al. (2004), the lower dispersion coefficient with increasing particle size (first peak ML 4 & SH 1) indicates that larger suspended particles are mainly channelled in the

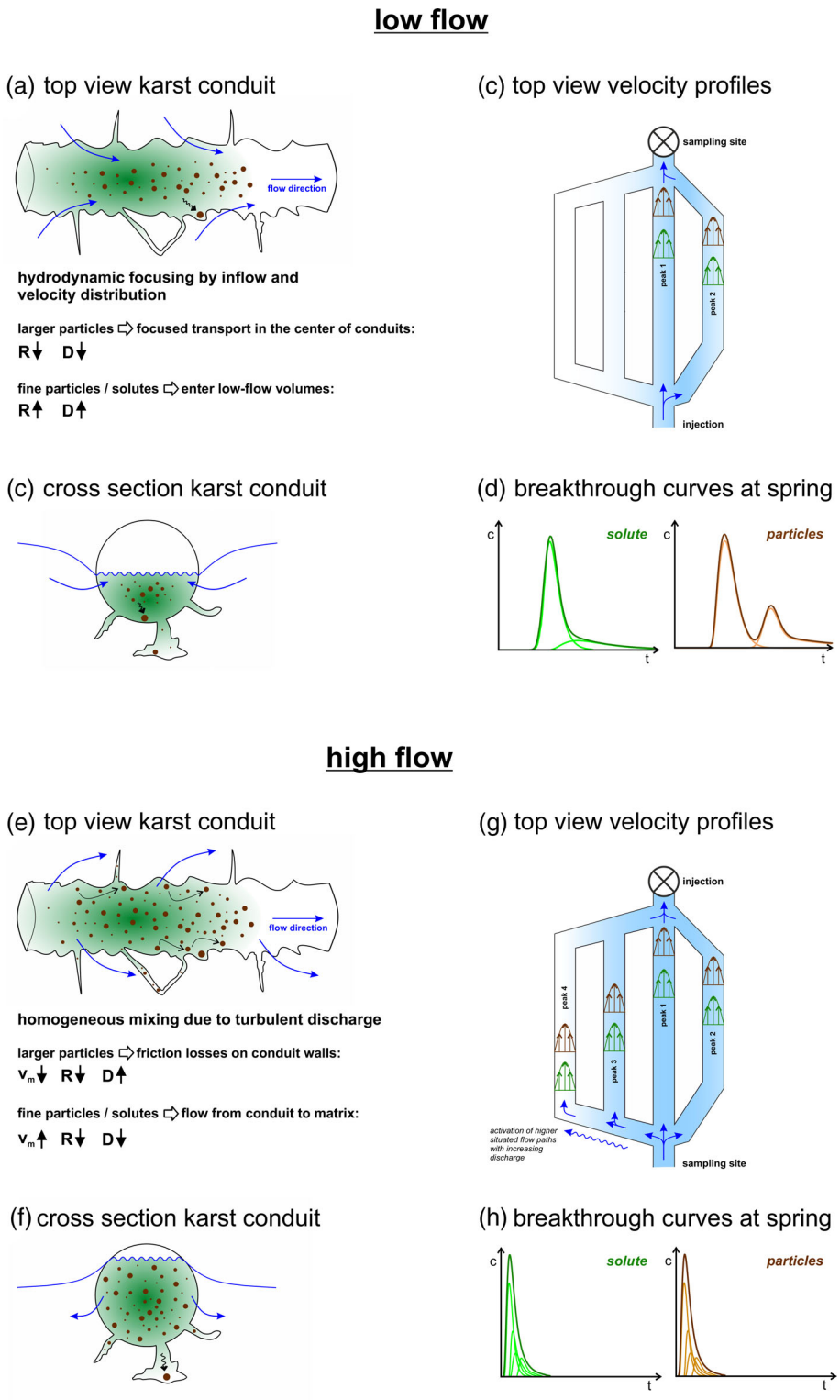

FIGURE 5 Concepts, illustrating the different transport behaviour of solutes (green) and suspended particles (brown) at low-flow (a–d) and high-flow (e–h) conditions. (a–d) Frictional losses at the edges are caused by fissure and cavity geometry of the conduits, drainage from the matrix into the conduit leading to hydrodynamic focusing. Larger particles are transported in the centre of conduits and are subject to sedimentation, while solutes are evenly spread in the entire pore space and matrix. The hydrodynamic focusing of suspended particles can highlight multiple flow paths, that are not visible in the BTC of the solute tracer because of its more dispersive transport. (e–f) More turbulent flow conditions result in a homogeneous mixing of large and small particles, and solutes. Increasing water pressure in the conduit due to increased runoff leads to increased infiltration into the fractures and pores of the limestone, and the activation of higher situated flow paths

centre of the conduits, move in faster streamlines, and have less diverse flow paths. In contrast, smaller particles can be transported more easily through a larger proportion of the entire conduit and enter the low-flow volumes of the adjacent fissured and porous rock matrix. This is in good agreement with the findings of Goeppert and Goldscheider (2019). They transferred these size exclusion processes, observed by Sirivithayapakorn and Keller (2003) and Auset and Keller (2004) for the pore scale in micromodels of porous media, to the dimensions of karst conduits with double porosity. At low-flow conditions, the hydrodynamic focusing of the suspended particles leads to less interaction between the centre of the karst conduit and the immobile regions, such as the adjacent fissures and matrix. Additionally, the immobile regions in karst result from eddies and pools. Therefore, the BTCs of the particle tracer for all size classes are narrow and show only very little tailing.

Although both tracers were injected with direct input into the water, recoveries of the small particles were only slightly lower than the recoveries for the dissolved tracer. The recoveries of the particles decrease with increasing size. Nevertheless, the observation of a lower recovery for particles compared with dissolved tracers at low-flow conditions is consistent with the results of other tracer experiments in karst systems (e.g., Auckenthaler et al., 2002) and gives countenance to the findings of Goeppert and Goldscheider (2008), who also measured higher solute tracer recoveries. Attenuation processes such as attachment to rocks and sedimentation influence particles, but not solutes. Furthermore, different processes as aggregation, straining, filtration and settling can affect the removal of particles (Schiperski et al., 2016).

As Ender et al. (2018) pointed out, that additional input from outside the cave system is very unlikely, and hydraulic conditions were constant, the data of this study indicate that the suspended particles travelled along preferential flow paths. Thus, these particles bypassed slower pathways and arrived slightly ahead of the conservative tracer; the particles diffused less in the fracture network or matrix. In addition, the hydrodynamic focusing to the centre of the conduit at low-flow conditions affects mainly particles, so that in total particles are transported faster than solutes through the conduit network (Figure 4). In contrast, solutes enter immobile or low-flow zones as carbonate rock matrix or fine fissures, leading to a tailing of the BTC. The observed skewness of the solutes can be related to the diffusion of the tracer to immobile water zones (Field & Pinsky, 2000). As hydrological conditions were constant during the tracer tests, remobilization of particles might have only a minor influence on the recoveries.

Hauns and Jeannin (1998) and Dewaide et al. (2018) linked a secondary peak to the presence of a pool in the conduit system, where the injected tracer might be trapped at the eddies, producing double-peaked BTCs. In this study, only the BTCs for the suspended particles show a double peak, but not the BTC for the conservative solutes. This is a highly peculiar finding, bus since we did not observe any additional input of sediments during the experiment, the double peaks can be attributed to the transport processes in the karst system. Conduit geometries are considered to have the strongest influence on the resulting BTCs of the suspended particles (Hauns et al., 2001; Massei et al., 2006). As both particle peaks seem to have a similar shape, they could be the result of two similar processes (Dewaide et al., 2018). The hydrodynamic focusing of particulate transport gives BTCs of particles a stronger temporal delineation. The existence of two consecutive flow paths in the conduit network can thus be visualized by particulate tracers in the form of multiple peaks at resurgences, which are not visible in the tailing of BTCs from solutes as their multiple peaks may hide in the smooth and skewed pattern. (Figure 5a–d).

4.2 | Conceptual model of solute and particle transport at high-flow

Overall, the discharge of the Ma Le cave system is characterized by high seasonal variability. It can be assumed that the hydraulic head within the conduits is greater than the head in the surrounding limestone at high-flow conditions. The increased water pressure in the karst conduits leads to infiltration into the fractures and pores of the limestone (Figure 5e,f) (Ford & Williams, 2013). The activation of additional flow paths by higher discharge increases the interaction of the water with the surfaces of the conduits (Massei et al., 2006).

The increased water level may lead to a reversal of the hydrodynamic focusing, resulting in a water flow from the conduit to the fissures and pores (Figure 5e,f). At high-flow conditions, the transport of particles is no longer channelled within the karst conduits but homogeneously distributed (Goeppert & Goldscheider, 2008); in more turbulent flow, particles are suspended over the whole water body (Atteia, 1998). Therefore, the interaction between conduit and matrix increases; larger fissure, cavity geometry (eddies, pools, siphons), and frictional forces at the conduit walls influence particles and can reduce the flow velocities of the larger particles. In immobile regions particles might settle, while solutes do not.

The results of this study indicate flow from the conduit into small fractures and fissures. But the results also show that the size of the suspended particles is of crucial importance for this process. The lower recoveries of the small particles (1–3 μm) demonstrate that these particles especially tend to infiltrate from the conduit into the fractured matrix and micro-fissures or attach to the rock surface due to the higher interaction energies. Small particles may also coagulate to larger particles (Atteia, 1998). Even attachment of small particles to larger ones might be a possible effect, reducing the recovery of small particles. Larger particles are influenced more by attenuation processes and gravitational sedimentation (Figure 5e,f). Due to these effects, the dispersion increases with increasing particle size, and the mean flow velocity decreases (Figure 4).

Due to the high flow velocities and the activation of additional flow paths, the individual BTCs are overlapping; singular peaks might merge into a single peak so that the individual flow paths can be detected neither with particle counters nor by analysing the solute tracer (Figure 5c,d,g,h). Therefore, the cumulative BTCs at the resurgence of the cave stream could cover the evidence of the single pathways, as visible for suspended particles at low-flow conditions.

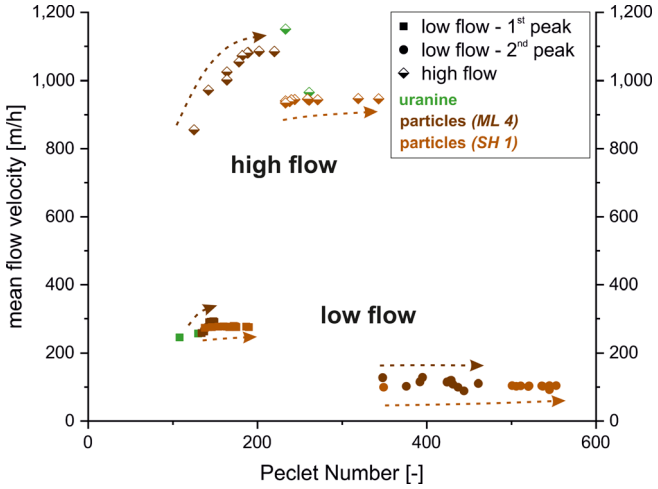

FIGURE 6 Two-dimensional plot of mean flow velocity and Péclet number evolution at different sites at high-flow and low-flow conditions depicting different hydrodynamic behaviours

Figure 6 shows the influence of the discharge on the transport dynamics and allows the characterization of the hydrodynamic behaviour of the different BTCs quantitatively. The results confirm contrasting behaviours at different hydraulic conditions. With increasing discharge in the conduit network, the ratio advection/dispersion becomes larger due to stronger increasing advection in comparison to the longitudinal dispersion. At high-flow conditions, the results reveal a very quick and advective transport in karst conduits with high dispersion and a high Péclet number. At low-flow conditions, both peaks of the BTCs reveal a still advective transport in the karst conduits, but with lower flow velocities. The higher Péclet numbers for the second peak indicate an increasing ratio of flow velocity to longitudinal dispersion for the additional flow path.

Dewaide et al. (2018) also found a second peak in their BTCs for tracer tests at constant hydraulic conditions in a karst system. As they calculated for their second peak a lower Péclet number (< 50) than for their first peak, they attributed their second peak to a slow and dispersive transport, caused by an underground lake. However, in this study, the Péclet number even rises for suspended particles in the second peak. So the transport is even more advective and cannot be caused by immobile zones or pools, but points to an additional flow path.

5 | CONCLUSION

This study compares the transport behaviour of a conservative solute and suspended sediment particles of different sizes in a cave system at low-flow and high-flow conditions. For this purpose, uranine and fine sediments were simultaneously injected into a swallow hole and sampled in the cave stream and at its resurgence.

By comparing BTCs of particles versus conservative solutes, the interaction with the surrounding matrix and hydrodynamic processes in the conduits can be deduced. Our results indicate a time shift in the tracer's breakthrough at low-flow conditions, arising from hydrodynamic focusing of the particles in karst conduits. Most of the suspended transport takes place in the centre of the conduits, where flow velocities are highest and retention is lowest. Therefore, flow velocities for particulate transport are higher than for solutes at low-flow conditions. A reversal of the conduit-matrix interaction and more turbulent flow conditions at a higher discharge leads to a more homogenous mixing of the tracers at high-flow conditions. Small particles and the solute show a similar transport through the cave system, while bigger particles are affected by attenuation processes and gravitational sedimentation.

When solutes are used as a tracer, multiple pathways in karst systems mostly lead to right-skewed BTCs with significant tailing, but only one visible peak. But with this study, injection of fine sediments allowed multiple flow paths to be identified with the double-peaked BTCs of the suspended particles at low-flow conditions (that cannot be attributed to any known other sediment source), while the BTC of the injected solute does not indicate a multiple path system. The preferential transport in the centre of karst conduits and the highly advective transport of the particles leads to narrow BTCs with separate peaks, while the more dispersive transport of solutes hides the multiple flow paths in the smooth tailing of the BTCs. At high-flow conditions, the activation of additional flow paths and the higher flow velocities might result in an overlapping of multiple peaks in the detected BTC, so that only one single, right-skewed peak is visible.

Several previous studies use the response to natural recharge events (snowmelt, rain events) or artificial tracer tests as an indicator for the characterization of karst aquifers. This study shows that the artificial injection of fine sediments as tracers may provide additional insights into flow path geometry in conduit-dominated systems, especially by comparing results of low-flow with high-flow conditions. When dealing with larger and more complex karst systems, this field experiment might reach its limitations. Nevertheless, our findings demonstrate a suitable approach and highlight the advantages of natural, local fine sediments as a tracer.

ACKNOWLEDGEMENTS

This project was funded by the German Federal Ministry of Education and Research (BMBF) (grant number 02WCL1415). The authors thank the whole sampling team, especially Nina Schwark, Joel Pompei, Niclas Danielzik, Patrick Keinarth, Ho Tien Chung, Doan The Anh, Tran Diep Anh and Nguyen Van Dong for their help during fieldwork. Big thanks to Oliver Dott for his support during the fieldwork and in processing the data. We are grateful to Markus Klotz for the good cooperation and thank him for providing particle counters. Thanks to the Belgian caving club SPEKUL for exploring and mapping the Ma Le cave system. Special thanks are given to Chloé Fandel for language checking the manuscript and for her valuable comments.

DATA AVAILABILITY STATEMENT

The data that support the findings of this study are available from the corresponding author upon reasonable request.

ORCID

Dominik Richter https://orcid.org/0000-0002-6140-5429

REFERENCES

Atteia, O. (1998). Evolution of size distributions of natural particles during aggregation: Modelling versus field results. *Colloids and Surfaces A: Physicochemical and Engineering Aspects*, *139*(2), 171–188. https://doi.org/10.1016/S0927-7757(98)00279-9

Auckenthaler, A., Raso, G., & Huggenberger, P. (2002). Particle transport in a karst aquifer: Natural and artificial tracer experiments with bacteria, bacteriophages and microspheres. *Water Science and Technology*, *46*(3), 131–138. https://doi.org/10.2166/wst.2002.0072

Auset, M., & Keller, A. A. (2004). Pore-scale processes that control dispersion of colloids in saturated porous media. *Water Resources Research*, *40*(3). https://doi.org/10.1029/2003WR002800

Bakalowicz, M. (2005). Karst groundwater: A challenge for new resources. *Hydrogeology Journal*, *13*, 148–160. https://doi.org/10.1007/s10040-004-0402-9

Behrens, H., Beims, U., Dieter, H., Dietze, G., Eikmann, T., Grummt, T., Hanisch, H., Henseling, H., Käss, W., Kerndorff, H., Leibundgut, C., Müller-Wegener, U., Rönnefahrt, I., Scharenberg, B., Schleyer, R., Schloz, W., & Tilkes, F. (2001). Toxicological and ecotoxicological assessment of water tracers. *Hydrogeology Journal*, *9*, 321–325. https://doi.org/10.1007/s100400100126

Carling, P. A., & McCahon, C. P. (1987). Natural siltation of brown trout (Salmo trutta L.) spawning gravels during low-flow conditions regulated streams. *Advances in Ecology*, 229–244.

Chen, Z., Auler, A. S., Bakalowicz, M., Drew, D., Griger, F., Hartmann, J., Jiang, G., Moosdorf, N., Richts, A., Stevanovic, Z., Veni, G., & Goldscheider, N. (2017). The world karst aquifer mapping project: Concept, mapping procedure and map of Europe. *Hydrogeology Journal*, *25*, 771–785. https://doi.org/10.1007/s10040-016-1519-3

Davies-Colley, R. J., Hickey, C. W., Quinn, J. M., & Ryan, P. A. (1992). Effects of clay discharges on streams. *Hydrobiologia*, *248*, 215–234. https://doi.org/10.1007/BF00006150

Dewaide, L., Bonniver, I., Rochez, G., & Hallet, V. (2016). Solute transport in heterogeneous karst systems: Dimensioning and estimation of the transport parameters via multi-sampling tracer-tests modelling using the OTIS (one-dimensional transport with inflow and storage) program. *Journal of Hydrology*, *534*, 567–578. https://doi.org/10.1016/j.jhydrol.2016.01.049

Dewaide, L., Collon, P., Poulain, A., Rochez, G., & Hallet, V. (2018). Double-peaked breakthrough curves as a consequence of solute transport through underground lakes: A case study of the Furfooz karst system, Belgium. *Hydrogeology Journal*, *26*, 641–650. https://doi.org/10.1007/s10040-017-1671-4

Dreybrodt, W. (1996). Principles of early development of karst conduits under natural and man-made conditions revealed by mathematical analysis of numerical models. *Water Resources Research*, *32*(9), 2923–2935. https://doi.org/10.1029/96WR01332

Dussart-Baptista, L., Massei, N., Dupont, J. P., & Jouenne, T. (2003). Transfer of bacteria-contaminated particles in a karst aquifer: Evolution of contaminated materials from a sinkhole to a spring. *Journal of Hydrology*, *284*(1), 285–295.

Ender, A., Goeppert, N., & Goldscheider, N. (2018). Spatial resolution of transport parameters in a subtropical karst conduit system during dry and wet seasons. *Hydrogeology Journal*, *26*, 2241–2255. https://doi.org/10.1007/s10040-018-1746-x

Field, M. S., & Leij, F. J. (2012). Solute transport in solution conduits exhibiting multi-peaked breakthrough curves. *Journal of Hydrology*, *440*, 26–35. https://doi.org/10.1016/j.jhydrol.2012.03.018

Field, M. S., & Pinsky, P. F. (2000). A two-region nonequilibrium model for solute transport in solution conduits in karst aquifers. *Journal of Contaminant Hydrology*, *44*, 329–351. https://doi.org/10.1016/S0169-7722(00)00099-1

Flynn, R., & Sinreich, M. (2010). Characterisation of virus transport and attenuation in epikarst using short pulse and prolonged injection multi-tracer testing. *Water Research*, *44*(4), 1138–1149. https://doi.org/10.1016/j.watres.2009.11.032

Ford, D., & Williams, P. (2013). Karst Hydrogeology. In *Karst hydrogeology and geomorphology*. John Wiley & Sons Ltd.

Frank, S., Goeppert, N., Ohmer, M., & Goldscheider, N. (2019). Sulfate variations as a natural tracer for conduit-matrix interaction in a complex karst aquifer. *Hydrological Processes*, *33*, 1292–1303.

Gale, S. J. (1984). The hydraulics of conduit flow in carbonate aquifers. *Journal of Hydrology*, *70*, 309–327.

Goeppert, N., & Goldscheider, N. (2008). Solute and colloid transport in karst conduits under low- and high-flow conditions. *Ground Water*, *46*, 61–68. https://doi.org/10.1111/j.1745-6584.2007.00373.x

Goeppert, N., & Goldscheider, N. (2019). Improved understanding of particle transport in karst groundwater using natural sediments as tracers. *Water Research*, *166*(2019), 115045. https://doi.org/10.1016/j.watres.2019.115045

Goldscheider, N., Chen, Z., Auler, A. S., Bakalowicz, M., Broda, S., Drew, D., Hartmann, J., Jiang, G., Moosdorf, N., Stevanovic, Z., & Veni, G. (2020). Global distribution of carbonate rocks and karst water resources. *Hydrogeology Journal*, *28*, 1661–1677. https://doi.org/10.1007/s10040-020-02139-5

Goldscheider, N., & Drew, D. (2007). Methods in karst hydrogeology. In *Tylor & Francis*. Leiden.

Goldscheider, N., Meiman, J., Pronk, M., & Smart, C. (2008). Tracer tests in karst hydrogeology and speleology. *Journal of Speleology*, *37*(1), 27–40.

Groves, C. (2007). *In: Goldscheider Nico, Drew David: Methods in karst hydrogeology*. Taylor & Francis Group.

Hauns, M., & Jeannin, P. Y. (1998). Tracer transport in underground rivers in karst: Tailing effect and channel geometry. *Bulletin d'Hydrogéologie*, *16*, 123–142.

Hauns, M., Jeannin, P. Y., & Atteia, O. (2001). Dispersion, retardation and scale effect in tracer breakthrough curves in karst conduit. *Journal of Hydrology*, *241*, 177–193. https://doi.org/10.1016/S0022-1694(00)00366-8

Hillebrand G (2008) *Transportverhalten kohäsiver Sedimente in turbulenten Strömungen – Untersuchungen im offenen Kreisgerinne*, (Dissertation), Karlsruhe Institute of Technology

Käss, W. (2004). *Geohydrologische Markierungstechnik*. Gebrüder Borntraeger.

Keller, A. A., Sirivithayapakorn, S., & Chrysikopoulos, C. V. (2004). Early breakthrough of colloids and bacteriophage MS2 in a water-saturated sand column. *Water Resources Research*, *40*(8). https://doi.org/10.1029/2003WR002676

Leibundgut, C., Maloszewski, P., & Külls, C. (2009). *Tracers in hydrology*. John Wiley & Sons, Ltd.

Mahler, B. J., Personne, J. C., Lods, G. F., & Drogue, C. (2000). Transport of free and particulate-associated bacteria in karst. *Journal of Hydrology*, *238*(3–4), 179–193. https://doi.org/10.1016/S0022-1694(00)00324-3

Mahler, B. J., Personné, J. C., Lynch, F. L., & van Metre, P. C. (2004). Sediment and sediment-associated contaminant transport through karst. In *Studies of cave sediments* (pp. 23–46). Springer. https://doi.org/10.1007/978-1-4419-9118-8_2

Massei, N., Wang, H. Q., Field, M. S., Dupont, J. P., Bakalowicz, M., & Rodet, J. (2006). Interpreting tracer breakthrough tailing in a conduit-dominated karstic aquifer. *Hydrogeology Journal*, *14*, 849–858. https://doi.org/10.1007/s10040-005-0010-3

McCarthy, J. F., & Zachara, J. M. (1989). Subsurface transport of contaminants. *Environmental Science & Technology*, *23*(5), 496–502.

Pronk, M., Goldscheider, N., & Zopfi, J. (2006). Dynamics and interaction of organic carbon, turbidity and bacteria in a karst aquifer system.

Hydrogeology Journal, *14*, 473–484. https://doi.org/10.1007/s10040-005-0454-5

Pronk, M., Goldscheider, N., Zopfi, J., & Zwahlen, F. (2009). Percolation and particle transport in the unsaturated zone of a karst aquifer. *Ground Water*, *47*(3), 361–369. https://doi.org/10.1111/j.1745-6584.2008.00509.x

Rügner, H., Schwientek, M., Milačič, R., Zuliani, T., Vidmar, J., Paunović, M., Laschoud, S., Kalogianni, E., Skoulikidis, N. T., Diamantini, E., Majone, B., Bellin, A., Chiogna, G., Martinez, E., López de Alda, M., Díaz-Cruz, M. S., & Grathwohl, P. (2019). Particle bound pollutants in rivers: Results from suspended sediment sampling in Globaqua River basins. *Science of the Total Environment*, *647*, 645–652. https://doi.org/10.1016/j.scitotenv.2018.08.027

Ryan, M., & Meiman, J. (1996). An examination of short-term variations in water quality at a karst spring in Kentucky. *Ground Water*, *34*(1), 23–30. https://doi.org/10.1111/j.1745-6584.1996.tb01861.x

Schillinger, J. E., & Gannon, J. J. (1985). Bacterial adsorption and suspended particles in urban Stormwater. *Journal of the Water Pollution Control Federation*, *57*(5), 384–389.

Schiperski, F., Zirlewagen, J., Hillebrand, O., Nödler, K., Licha, T., & Scheytt, T. (2015). Relationship between organic micropollutants and hydro-sedimentary processes at a karst spring in south-West Germany. *Science of the Total Environment*, *532*, 360–367. https://doi.org/10.1016/j.scitotenv.2015.06.007

Schiperski, F., Zirlewagen, J., & Scheytt, T. (2016). Transport and attenuation of particles of different density and surface charge: A karst aquifer Field study. *Environmental Science and Technology*, *50*, 8028–8035. https://doi.org/10.1021/acs.est.6b00335

Sinreich, M., Flynn, R., & Zopfi, J. (2009). Use of particulate surrogates for assessing microbial mobility in subsurface ecosystems. *Hydrogeology Journal*, *17*, 49–59. https://doi.org/10.1007/s10040-008-0362-6

Sirivithayapakorn, S., & Keller, A. (2003). Transport of colloids in unsaturated porous media: A pore-scale observation of processes during the dissolution of air-water interface. *Water Resources Research*, *39*(12), 1346. https://doi.org/10.1029/2003WR002487

Toride, N., Leij, F. J., & van Genuchten, M. T. (1993). A comprehensive set of analytical solutions for nonequilibrium solute transport with first-order decay and zero-order production. *Water Resources Research*, *29*(7), 2167–2182. https://doi.org/10.1029/93WR00496

Toride N, Leij FJ & van Genuchten MT (1999) The CXTFIT code for estimating transport parameters from laboratory or field tracer experiments, *research port no. 137 US salinity laboratory*, *Riverside, CA*

Vesper, D., & White, W. B. (2003). Metal transport to karst springs during storm flow: An example from Fort Campbell, Kentucky/Tennessee, USA. *Journal of Hydrology*, *276*(1–4), 20–36. https://doi.org/10.1016/S0022-1694(03)00023-4

Vuilleumier, C. (2017). *Hydraulics and sedimentary processes in the karst aquifer of Milandre (Jura Mountains, Switzerland)*. University of Neuchatel.

SUPPORTING INFORMATION

Additional supporting information may be found in the online version of the article at the publisher's website.

How to cite this article: Richter, D., Goeppert, N., & Goldscheider, N. (2022). New insights into particle transport in karst conduits using comparative tracer tests with natural sediments and solutes during low-flow and high-flow conditions. *Hydrological Processes*, *36*(1), e14472. https://doi.org/10.1002/hyp.14472